

# Interplay of point defects, extended defects, and carrier localization in the efficiency droop of InGaN quantum wells light-emitting diodes investigated using spatially resolved electroluminescence and photoluminescence

Yue Lin,<sup>1,2,3,a)</sup> Yong Zhang,<sup>1,b)</sup> Zhiqiang Liu,<sup>4</sup> Liqin Su,<sup>1</sup> Jihong Zhang,<sup>3</sup> Tongbo Wei,<sup>4</sup> and Zhong Chen<sup>3</sup>

<sup>1</sup>Electrical and Computer Engineering Department and Energy Production and Infrastructure Center, University of North Carolina at Charlotte, Charlotte, North Carolina 28223, USA

<sup>2</sup>Fujian Institute of Research on the Structure of Matter, Chinese Academy of Sciences, Fuzhou, Fujian 350002, People's Republic of China

<sup>3</sup>Department of Electronic Science and Fujian Engineering Research Center for Solid-State Lighting, Xiamen University, Xiamen, Fujian 361005, People's Republic of China

<sup>4</sup>R&D Center for Semiconductor Lighting, Chinese Academy of Sciences, Beijing 100083, People's Republic of China

(Received 22 October 2013; accepted 17 December 2013; published online 10 January 2014)

We perform both spatially resolved electroluminescence (SREL) as a function of injection current and spatially resolved photoluminescence (SRPL) as a function of excitation power on InGaN quantum well blue light-emitting diodes to investigate the underlying physics for the phenomenon of the external quantum efficiency (EQE) droop. SREL allows us to study two most commonly observed but distinctly different droop behaviors on a single device, minimizing the ambiguity trying to compare independently fabricated devices. Two representative devices are studied: one with macroscopic scale material non-uniformity, the other being macroscopically uniform, but both with microscopic scale fluctuations. We suggest that the EQE–current curve reflects the interplay of three effects: nonradiative recombination through point defects, carrier localization due to either In composition or well width fluctuation, and nonradiative recombination of the extended defects, which is common to various optoelectronic devices. By comparing SREL and SRPL, two very different excitation/detection modes, we show that individual singular sites exhibiting either particularly strong or weak emission in SRPL do not usually play any significant and direct role in the EQE droop. We introduce a two-level model that can capture the basic physical processes that dictate the EQE–current dependence and describe the whole operating range of the device from 0.01 to 100 A/cm<sup>2</sup>. © 2014 AIP Publishing LLC. [<http://dx.doi.org/10.1063/1.4861150>]

## I. INTRODUCTION

Solid-state lighting (SSL) technology is progressing rapidly in recent years, and light-emitting diodes (LEDs) have now been used in many commercial areas.<sup>1</sup> However, for general illumination applications, major improvement is still needed in areas such as energy conversion efficiency and the ability to operate efficiently under high current condition. Typical LEDs based on InGaN quantum wells face the so-called “current droop” in electroluminescence (EL),<sup>2–4</sup> namely, with increasing the forward driving current  $I_f$ , the external quantum efficiency (EQE) initially increases and then decreases after reaching a peak at  $I_{max}$ . EQE is defined as the ratio of the number of the photons emitted and extracted to that of the electrons injected. A number of intrinsic and extrinsic mechanisms have been proposed to explain the droop effect, including (1) Auger recombination,<sup>5–11</sup> (2) carrier leakage [i.e., carriers “spill over” the InGaN quantum wells (QWs)] that itself may be due to various possibilities: difference in mobility between electrons and holes, polarization field, and insufficient electron blocking between the active region and p-GaN layer at high injection level,<sup>2,12–18</sup>

(3) density activated defect recombination (DADR);<sup>19,20</sup> and (4) carrier delocalization (CDL).<sup>21–26</sup> The last two mechanisms, DADR and CDL, share the same general idea: at low current levels, the carriers populate the lower energy regions where the radiative recombination dominates whereas at high current levels, the carriers start to populate the high energy regions where nonradiative loss is more prominent. However, the energy states involved are somewhat different. In CDL, the lower energy regions, local energy minimums (LEMs), may correspond to either those In rich regions caused by the In composition fluctuation or well width fluctuation;<sup>19–26</sup> in DADR, the higher energy regions are assumed to be more defected.<sup>21</sup> We would like to point out that lower emission efficiency does not necessarily mean higher density of defects, instead may simply be due to the higher carrier mobility that makes the defects more detrimental.<sup>27,28</sup> Specifically, it is the lower carrier mobility of the lower energy states that makes the carriers at these states more immune from the nonradiative defect centers. Therefore, for a material with a given density of nonradiative defect states, the mechanism of the EQE droop is expected to sensitively depend on the uniformity of the material (well width and In composition), and it is unrealistic trying to identify a single universal primary droop mechanism for different types of materials and devices.

<sup>a)</sup>yuelin@fjirsm.ac.cn

<sup>b)</sup>yong.zhang@uncc.edu

In the literature, the EQE- $I_f$  curves are found in various shapes although each shows a maximum EQE at  $I_{max}$ .<sup>21,29,30</sup> We have recently proposed to use two parameters to characterize them:<sup>31</sup> the initial increase rate  $\tau_r$  of the EQE before reaching the maximum, and the droop rate  $\tau_{EQE}$ . The process resembles the time-resolved photoluminescence (TPL) where the rise and decay times jointly determine the maximum intensity point.<sup>32</sup> The two most noticeable types of the EQE- $I_f$  curves in the literature are type I, exhibiting a slow rise and a slow decay; type II, exhibiting a fast rise and a fast decay. Because the rise portion of the curve reflects how fast the nonradiative defects can be saturated, the ideal scenario should really have a large  $\tau_r$  and small  $\tau_{EQE}$ , which may be referred to as type III and will yield a high peak EQE at a small  $I_{max}$ , instead of a large  $I_{max}$  as often suggested to be favorable in the literature. We have recently reported a spatially resolved electroluminescence (SREL) study on an InGaN LED with macroscopic material inhomogeneity, which allowed us to probe both type I and type II droop behaviors simultaneously on a single device.<sup>31</sup> This study has revealed that in the area with significant localization, the localization effect leads to a large  $\tau_r$  or small  $I_{max}$ , high peak EQE, large initial  $\tau_{EQE}$ , and preserves the higher EQE for the portion of the carriers that remains localized at the high current level (e.g., 100 A/cm<sup>2</sup>) whereas in the area lacking the significant localization of the same device, a small  $\tau_r$  or large  $I_{max}$ , smaller  $\tau_{EQE}$ , but low EQE at the high current level were observed. We have further pointed out that point defects (PDs), instead of extended defects (EDs), play the major role in the rising portion of the curve<sup>31</sup> by noticing the generally different roles of PDs and EDs in carrier diffusion and recombination.<sup>28</sup>

In the literature, the study of the droop effect was typically performed on a macroscopic size device and thus yielded a spatially averaged effect over regions that may behave very differently in the efficiency droop. The conventional practice in the droop study is to compare devices with selective changes in the device structure, assuming that everything else remains the same, for instance changing the substrate type to examine the polarization effect. In contrast, the spatially resolved droop study of this work allows us to examine primarily the effect of the spatial variation or inhomogeneity of the active layer (InGaN) on the droop effect in the same device structure (such as substrate, contacts, and light extraction efficiency) and, thus, minimizes the potential ambiguity related to the variations in device structure and fabrication that involve a large number of layers and processes. Therefore, a spatially resolved study on the droop effect is expected to provide unique insights into the droop mechanism and the directions for overcoming it.

Spatially resolved optical spectroscopy methods are often used for investigating the mechanism of carrier localization to the LEM, for instance, recent efforts using spatially resolved photoluminescence (SRPL),<sup>33</sup> and both SREL and SRPL<sup>34</sup> in InGaN QW green LEDs. As observed in virtually all other semiconductor QW structures involving alloys, both alloy and well width fluctuation are also found to contribute to the localization effect in the InGaN QW LEDs<sup>34</sup> although the details are sensitive to the specific

growth conditions. In this work, we apply both SREL and SRPL to InGaN QW blue LEDs to investigate how the localization may affect the droop, the correlation of results from the two rather different types of spatially resolved techniques, and the relevancy of the  $\mu$ -PL result to the droop behavior. Note that our focus is not on the determination of the specific localization mechanism (namely well width fluctuation vs. In composition fluctuation) on a particular device, but the effect of the localization on the droop, because the effects of these two mechanisms are qualitatively similar, at least in EL, which will be illustrated later. In our recent work,<sup>31</sup> the discussions were focused on one particular device in which two distinctly different droop behaviors, typically reported on two independent devices in the literature, were observed on one device because of the unintended macroscopic inhomogeneity of the material. In this work, we include another representative device of which the material is in general very uniform in a macroscopic scale but with microscopic singular regions showing lower EQEs. It is of great interest to find out whether or not such a lower efficiency region droops differently from the general area. Based on the observations made on the two devices, more insights are provided to the mechanism of the droop in the InGaN LED and to the generally observed performance degradation in other optoelectronic devices, such as solar cells under high concentration and semiconductor lasers under high current.

## II. EXPERIMENT

We have investigated two LEDs with similar structures, except that one is grown on a free-standing GaN substrate, device A, and the other on a c-plane sapphire substrate, device B. Device A includes, from bottom to top, 2  $\mu$ m undoped GaN, 2  $\mu$ m n-GaN, buffer layer with 3 InGaN/GaN QWs (1 nm/30 nm), 5 QWs with doped barriers (3 nm/8 nm), 6 active QWs (3 nm/8 nm), 40 nm AlGaIn, and 150 nm p-GaN. Device B has very similar structures except for some minor differences, for instance, the p-GaN layer is thicker. The area of the active region is 1 mm<sup>2</sup>. The details of device fabricating can be found elsewhere.<sup>35</sup> One apparent difference between the two devices is that the defect density is  $\sim 10^7$  cm<sup>-2</sup> for A and  $\sim 10^8$  cm<sup>-2</sup> for B, presumably due to the difference in substrate. As typical in the literature, the defect densities quoted here are for the EDs (typically threading dislocations). The concentrations of the PDs, which could be as important, are unknown, as usual. Note that these two devices are not used for comparing their device performance, but represent two distinctly different cases in the uniformity of the active layer. However, we note that despite the substantially lower ED density in the material of the device A, the peak EQE of A in either macroscopic or spatially resolved measurement is found to be lower than those of B, showing the potential ambiguity of making comparison between two independent devices. The substrate difference is unlikely responsible for the difference in the material uniformity between the two devices but other subtle differences in the growth conditions are. For this work, device A provides a unique opportunity for us to investigate

the two distinctly different types of droop in a way that might not be possible otherwise (even SREL were performed); device B allows us to compare the droop in a single device between the general area and the isolated singular region with lower efficiency.

The  $\mu$ -EL and  $\mu$ -PL spectra were measured using a Horiba LabRAM HR confocal optical system. A Keithley 2401 source unit and a 325-nm UV laser were used as excitation sources, respectively, for EL and PL. EL and PL mappings were performed using a  $40\times$  UV objective lens with  $NA=0.5$  with a diffraction limit spatial resolution approximately 550 nm at emission wavelength 450 nm. For PL, the excitation spot size is approximately 800 nm. The same device area is mapped for EL and PL, thus, offering a direct comparison between two different excitation modes that involve distinctly different physics processes. PL excitation power varied from 0.055 to 5.5 mW, approximately corresponding to  $1\times(10^4\text{--}10^6)$  W/cm<sup>2</sup> in density or  $1.6\times(10^{22}\text{--}10^{24})$  cm<sup>-2</sup> s<sup>-1</sup> in photon flux. EL driving current varied from 0.1 to 950 mA or 0.01 to 95 A/cm<sup>2</sup>, which corresponds to an average injection carrier flux of  $6.3\times 10^{16}\text{--}5.9\times 10^{20}$  cm<sup>-2</sup> s<sup>-1</sup>.

Both devices have no encapsulation because of using a short working distance microscope lens. The peak EQE of device B is  $\sim 34\%$ , which corresponds to an approximate internal quantum efficiency  $\geq 68\%$ , a rather decent value for room temperature,<sup>36</sup> if we consider the extraction efficiency of such a “naked” device is likely below 50%.<sup>37</sup> A nominally same chip was found to have 44% EQE after encapsulation.<sup>7</sup> Although devices with substantially higher peak EQE have been reported in the literature, for instance, 77.4% with patterned substrate and specially designed electrodes, the “standard” device of the same material was reported to have 54.4% EQE.<sup>38</sup> Moreover the 54.4% device also showed a very low droop rate,  $\tau_{\text{EQE}}\sim 0.15\%/(\text{A}/\text{cm}^2)$ , among the best reported in the literature. Therefore, the devices investigated in this work fall into the category of the better than average

performance. Most droop studies have been performed on the devices of this category, and thus most improvement is needed for them.

Although the primary EL data of device A have been reported in a recent publication,<sup>31</sup> they are included with more details in this work for comparison with the PL mapping data of the same device, and data of the device B.

### III. RESULTS AND DISCUSSIONS

#### A. Electroluminescence and photoluminescence mapping

Figure 1 shows the EL images taken by a digital camera for the two devices under different forward currents: Figs. 1(a)–1(c) for device A under 0.5, 3, and 100 mA, respectively, and Figs. 1(d)–1(f) for device B under the same currents. One can clearly see that for device A, at low current, only isolated spots and regions emit weakly. With increasing current, the emitting regions expand and some gradually merge into each other. However, some areas remain relatively dark or emit only weakly even under high current. This device appears to be highly non-uniform. Note that the bright and dark regions often appear in a macroscopic size (as large as tens of microns) that far exceeds the typical carrier diffusion length in this type of material, typically a few hundred nm. Therefore, they are practically independent. In contrast, for device B, the emission is much more uniform under all current levels.

Spatial mappings of the EL and PL emission spectra from a same area were performed for both devices. Figure 2 shows the intensity and peak energy distributions for device A in an area of  $16\ \mu\text{m}\times 20\ \mu\text{m}$ , and Figure 3 for device B of  $10\ \mu\text{m}\times 10\ \mu\text{m}$ , where PL were obtained under 0.55 mW excitation and EL under  $I_f=5$  mA. Similar to the optical images of Fig. 1, device A exhibits much more significant macroscopic scale spatial variation than device B in both PL and EL intensity. Figure 4 shows the typical EL spectra

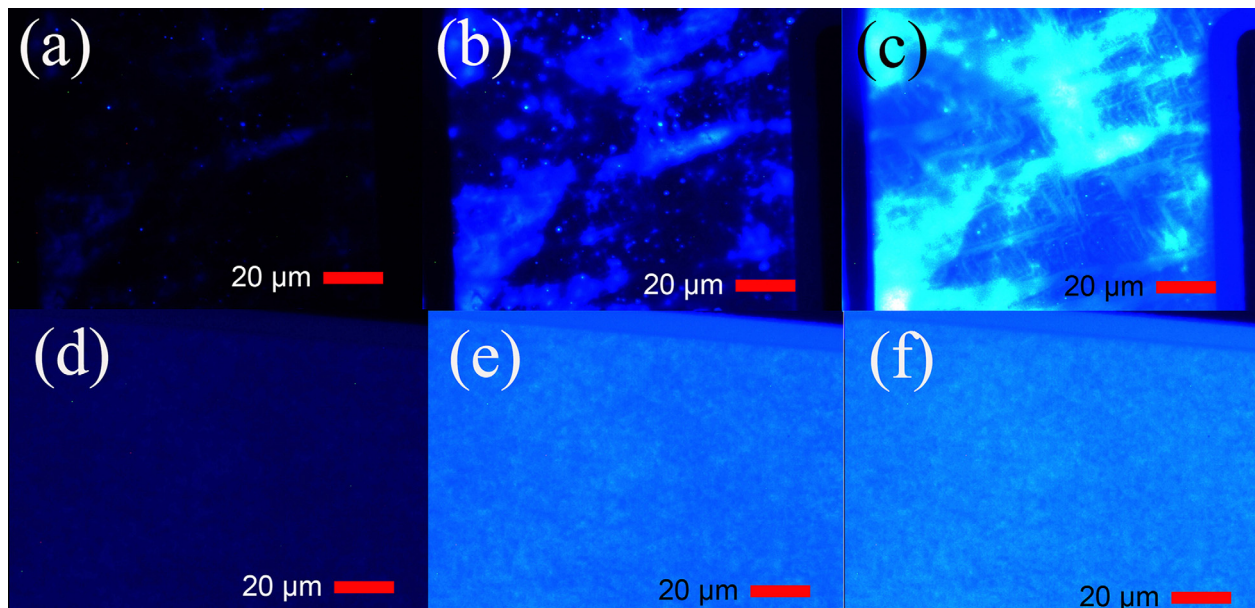


FIG. 1. The photo images of LEDs operated under different forward currents: 0.5 mA, 3 mA, 100 mA (a)–(c) for device A and (d)–(e) for device B.

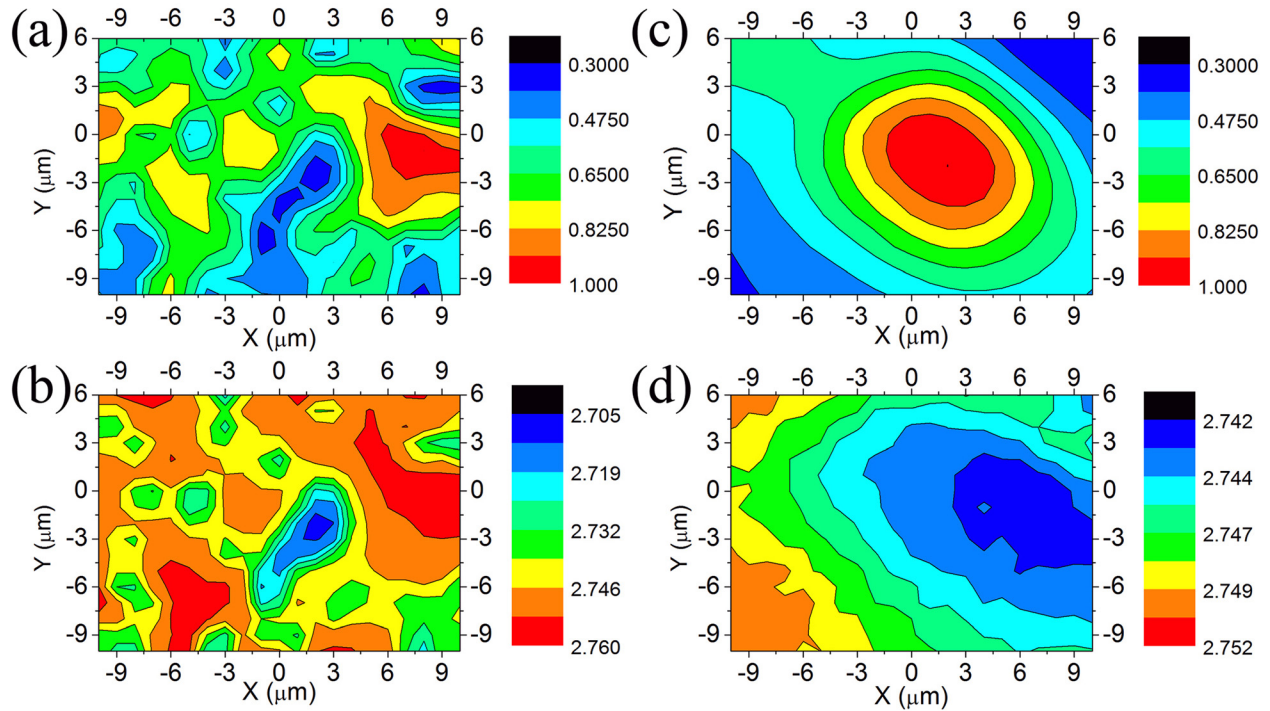


FIG. 2. PL (under 0.55 mW) and EL (under  $I_f=5$  mA) mapping results of device A of the same area: (a) PL intensity; (b) PL peak-energy; (c) EL intensity; (d) EL peak-energy. The intensity is the integration over the spectral range of 2.64–2.80 eV. Note that the energy scales are different between (b) and (d).

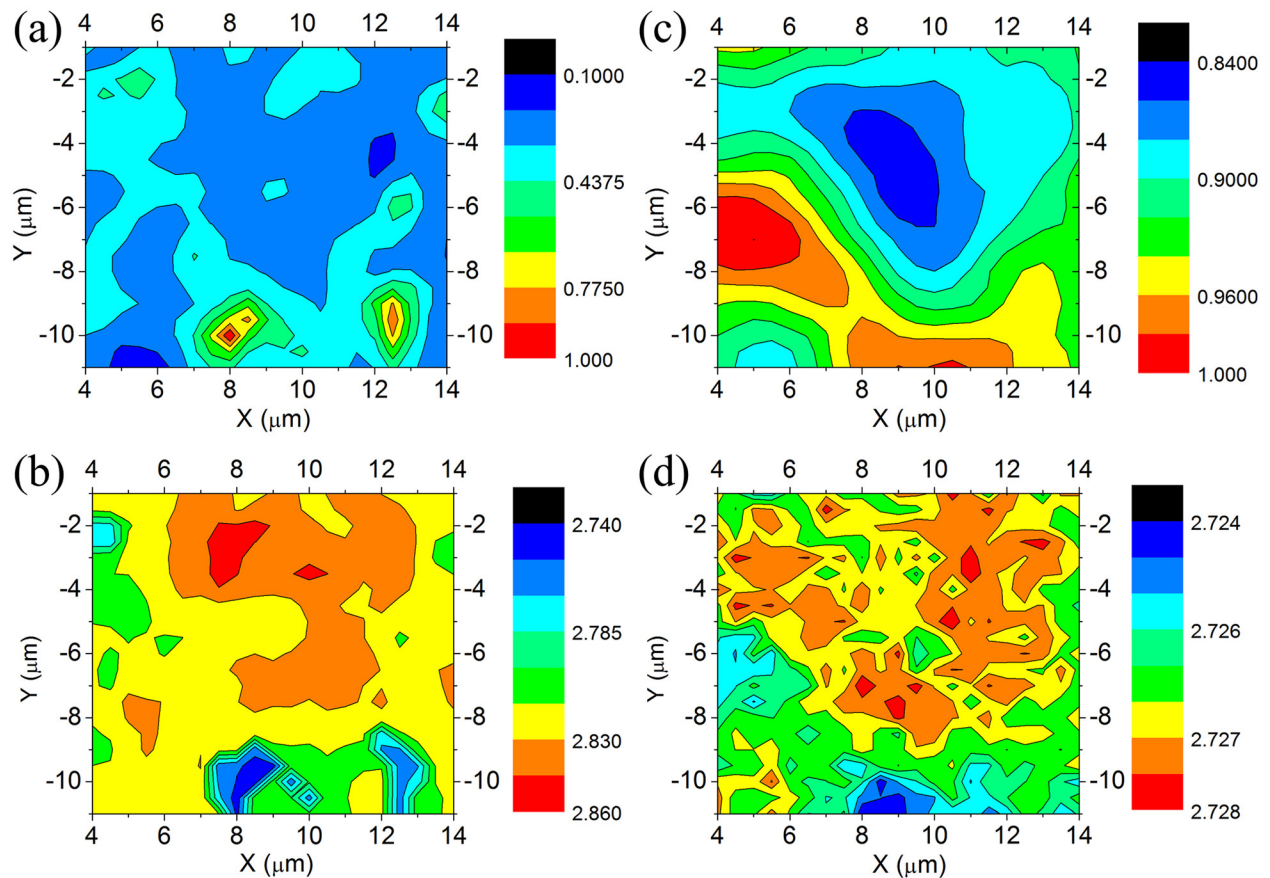


FIG. 3. PL (under 0.55 mW) and EL (under  $I_f=5$  mA) mapping results of device B of the same area: (a) PL intensity; (b) PL peak-energy; (c) EL intensity; (d) EL peak-energy.

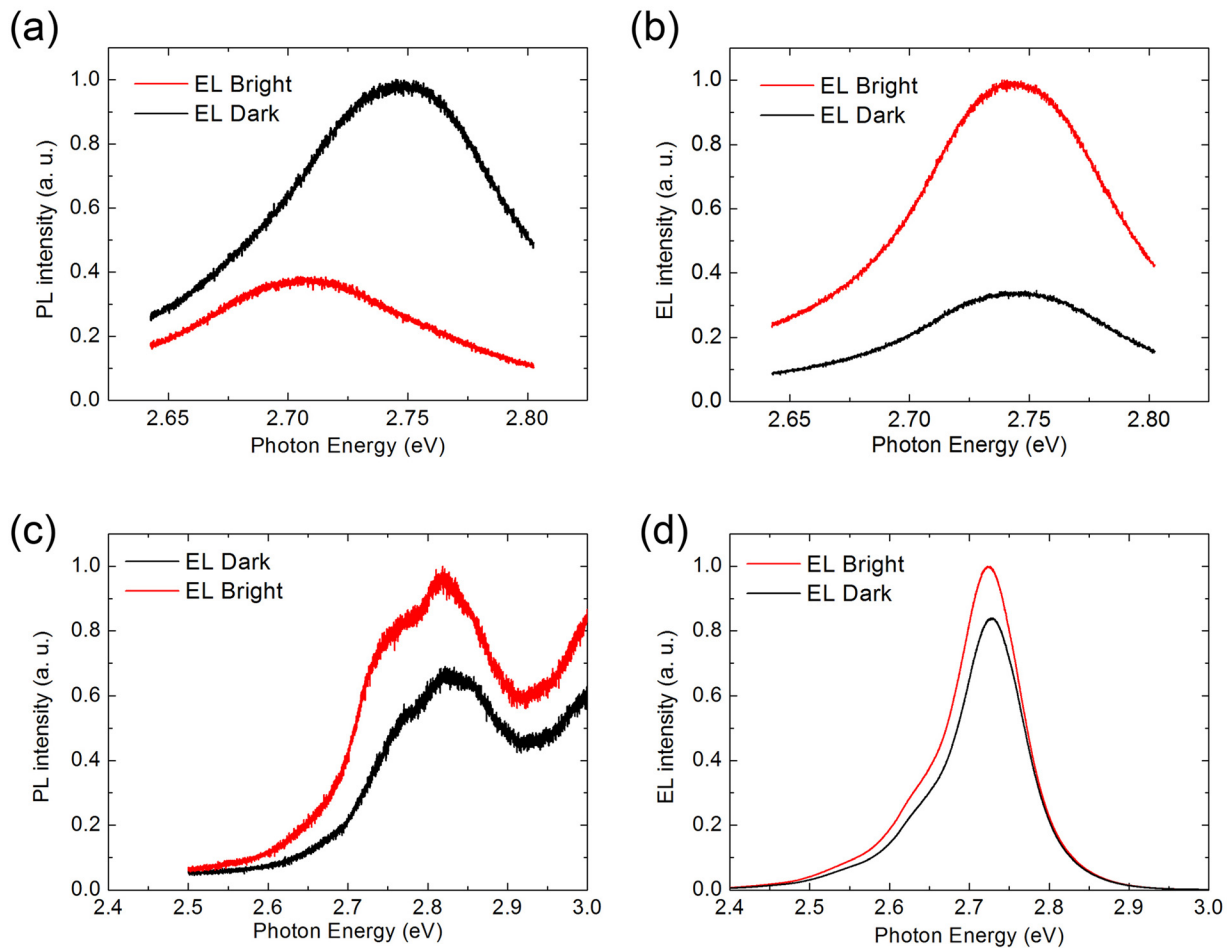


FIG. 4. PL and EL spectra measured from the same bright and dark spots of EL: (a) PL and (b) EL of sample A; (c) PL and (d) EL of sample B. PL spectra are measured under 5 mW laser power and EL are taken under 5 mA forward current.

under  $I_f = 5$  mA for the dark and bright regions, compared to the PL under  $\sim 10^6$  W/cm<sup>2</sup> from the same regions. The intensity variation between the dark and bright regions is much larger, 80%–90%, for device A than that for device B, only 10%–20%. These two devices are the representatives of two distinctly different situations.

We first discuss device A. The mapping results showed in Figs. 2(a)–2(d) are, respectively, for PL intensity, PL peak-energy, EL intensity, and EL peak-energy. For PL, there is a general correlation between PL intensity—Fig. 2(a) and peak energy—Fig. 2(b): specifically, the intensity minimum largely matching the peak energy minimum, which seems to be consistent with the case reported in the literature:<sup>39</sup> a region with higher In concentration, thus, lower peak energy, tends to have higher PD density. For a region with a larger well width thus lower energy, the PL intensity is expected to be higher because the well width fluctuation usually does not introduce additional nonradiative defects. Although SRPL has been shown to be very helpful in assessing the material uniformity and identifying the carrier localization sites, we show that SREL is in fact more relevant to the actual device performance. Comparing the EL and PL mapping data, we have found two seemingly contradicting observations: (1) in EL ( $I_f < I_{max}$ ), Figs. 2(c) and 2(d) show an anti-correlation between the emission intensity and peak

energy. (2) A bright spot in EL may correspond to a dark spot in PL with lower peak energy, which is evident comparing Fig. 2(a) with Fig. 2(c), or Fig. 4(a) with Fig. 4(b). The apparent paradoxical difference between the PL and EL mapping is in fact fully understandable. Although in both cases the emission is measured locally (local collection), there is a distinct difference between their excitation modes: PL mapping is under local excitation and local collection, thus the intensity is directly related to the local non-radiative recombination center density whereas EL mapping is under nearly homogeneous excitation (via carrier injection), but also under local collection. It is probably reasonable to assume homogeneous injection for both electrons and holes from n-GaN and p-GaN, respectively, but the carrier distributions could nevertheless be non-uniform in the QW layers. Based on the fact that the EL peak energies are rather close to each other between the bright and dark regions, as shown in Fig. 2(d), one can assume that the average In composition remains more or less the same throughout the whole InGaN layer although on the microscopic scale, the In composition distributions could be rather different between the bright and dark regions. In fact, the PL peak energy of the EL bright region in Fig. 4(a) corresponds to a lower energy shoulder in EL at very low current ( $< 5$  mA), presumably due to In segregation. We suggest that in this device, the EL bright region

exhibits more microscopic In segregations, providing the carrier trapping and collection sites, whereas in the EL dark region the In distribution is more uniform, thus lacking the ability to trap and collect the carriers. In the case of the local excitation mode in PL, the emission peak energy and intensity reveal, respectively, the local energy states and radiative recombination efficiency. Because the In-rich region could be more defective and the achieved effective excitation density was relatively low, the EL bright region instead appears to be dark in the PL mapping. However, under homogeneous excitation of EL, because of the carrier diffusion and accumulation, nonradiative defects at the In-rich sites are easily saturated even at a relatively low current level, leading to stronger emission.

The distributions as well as the magnitude of the variation in the peak energy are somewhat different between PL, Fig. 2(b), and EL, Fig. 2(d). The spatial variation of the peak energy is substantially smaller for EL,  $\sim 35$  meV vs.  $\sim 60$  meV for PL. The difference could be due to the fact that in EL the average carrier density even under the lowest current is already much higher than the local carrier density in PL. This is because that most absorption occurs in the much thicker GaN layers and most carriers recombine before reaching the QWs, and also because of the lateral carrier diffusion from the excitation site and the surface reflection loss. Therefore, the state filling effect is much more significant in EL, which is also evident in Figs. 4(a) and 4(b) where the state filling effect in PL is weaker for the EL bright spot than for the EL dark spot. Figure 5 shows the energy shifts for the typical EL bright and dark spots with varying  $I_f$  and compared to the shifts for the same spots in PL. Consistent with the PL mapping in Fig. 2 as well as the typical PL spectra shown in Fig. 4(a), the PL peak positions showed in Fig. 5(a) confirm that the bright region of EL indeed has some LEMs, thus showing lower emission energy than the dark region. For the EL peak energies shown in Fig. 5(b), the initial small red shifts (only a few meV) at low current are likely due to the saturation of some weakly localized states, and the blue shifts at high current should be associated with the state filling effect that is closely related to the EQE droop, which will be discussed later. For this device, it is apparent that the spatial variation of the  $\mu$ -PL and  $\mu$ -EL intensity data do not correlate, in fact almost anti-correlate, with each other, i.e., a region of high PL intensity may show a low EL intensity, and vice versa. Therefore, the  $\mu$ -PL data are not always reliable and useful

in predicting the EL behavior of the device. Note that in Fig. 5(b), the peak energy of the EL bright region is slightly higher than that of dark region although the reverse is typically found in the mapping data Fig. 2(d). The small variation in the absolute transition energy at low current could be simply due to the In composition variation between the two macroscopically separated regions. The important contrast between the bright and dark regions lies in the difference in their energy shifts with increasing current, i.e., the bright region exhibits more energy fluctuation thus more localization effect than the dark region.

We now discuss the results for device B. As shown in Figs. 3(c) and 3(d), the spatial variations in emission intensity ( $\sim 15\%$ ) and peak energy ( $\sim 5$  meV) in EL are much smaller than those of device A. Similar to device A, there is in general anti-correlation between the EL intensity and peak energy, but the peak energy variation is very small (merely a few meV), indicating fairly good material uniformity. However, in contrast to device A, the anti-correlation between the intensity and peak energy is also found in the PL mapping, as shown in Figs. 3(a) and 3(b), and the spatial variation in PL intensity is also smaller than that in device A, if we neglect a few isolated particularly bright spots. Similar to device A, there are finer scale (beyond our spatial resolution) energy fluctuations or LEMs that yield a lower energy shoulder in EL spectra, as revealed in Fig. 4(d). It is these LEMs that play a key role in the droop, which will be discussed in Sec. III B. For those bright spots about  $1 \mu\text{m}$  in size in the PL mapping, the anti-correlation between the intensity and peak energy is most apparent, which is in fact consistent with the expectation that a lower energy or localized state tends to have a higher emission efficiency. These spots likely correspond to the regions of larger well widths.<sup>40</sup> However, these bright PL spots show only average intensity in the EL mapping because they behave like small puddles readily to be filled by the carriers even under a moderate injection level. For the dark spot in the EL mapping [Fig. 3(c)], the EL spectrum looks nearly the same as that of the bright spot except for the intensity difference [Fig. 4(d)]. Furthermore, the PL spectra of the EL bright and dark spots are also very similar but different in intensity [Fig. 4(c)]. Again in device B, those sub- $\mu\text{m}$  or  $\mu\text{m}$  scale dark or bright spots observed in the PL mapping do not have much impact on the EL performance or droop once the current is moderately high, for instance,  $5 \text{ mA}$  or  $0.5 \text{ A/cm}^2$ .

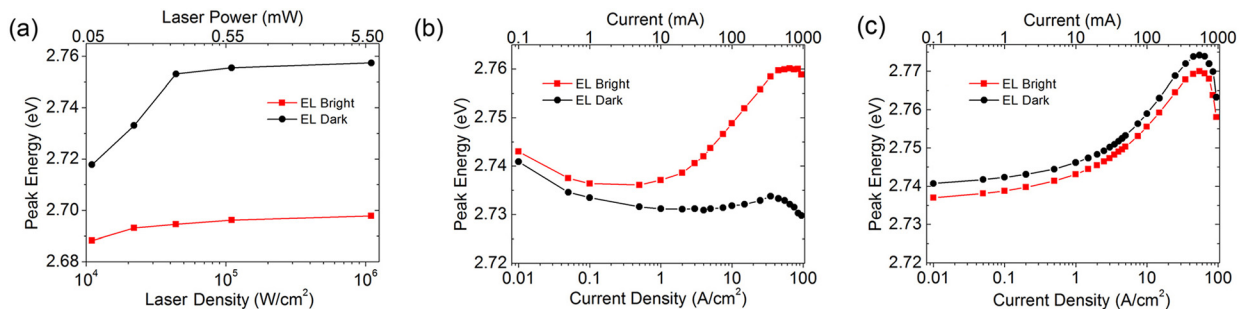


FIG. 5. The PL and EL peak-energy shifts for the EL bright and dark regions: (a) for PL of device A, (b) for EL of device A, and (c) for EL of device B.

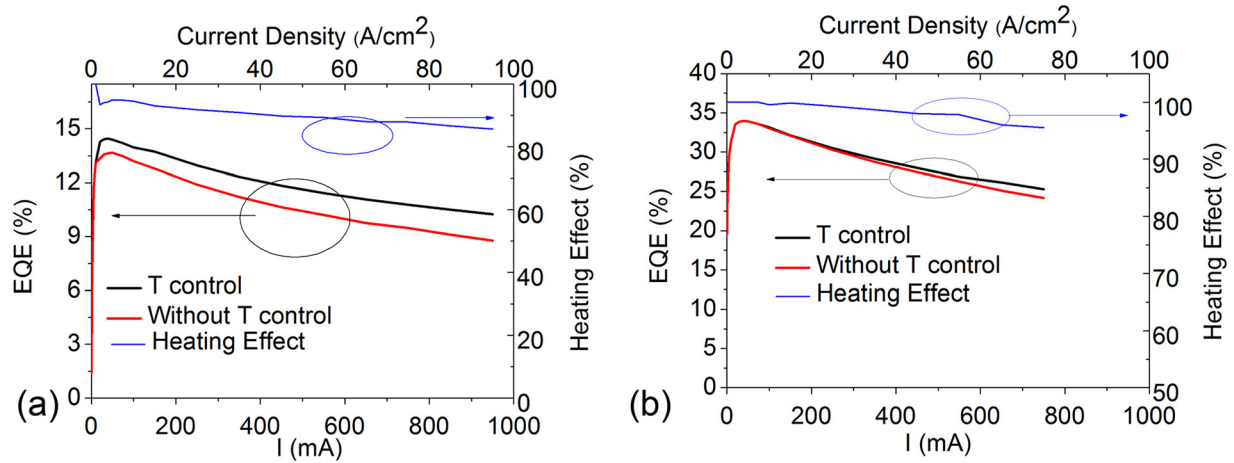


FIG. 6. The EQE droop curves with and without junction temperature control. The junction temperature was set to 35 °C for the controlled case. The right axis shows the ratio of the two curves—heating effect (a) for device A and (b) for device B.

## B. Spatially resolved EQE droop

We next discuss the spatial variation of the efficiency droop for the two devices. As typically done in the literature, we have first measured the EQE vs.  $I_f$  for the whole device, with the results shown in Figure 6. Device B appears to be more than twice as efficient as device A, despite it was grown on a sapphire substrate with a higher ED density. However, if we take into account the fact that roughly half of the area of device A is rather inefficient, as revealed in Fig. 1, the EQE of the bright region of device A is in fact comparable to that of device B, which will be apparent later in the study of the spatially resolved droop. These observations indicate that, on the one hand, making comparison between two nominally same structures with the assumption only changing the substrate could be problematic; on the other hand, the spatially averaged data might not reveal an accurate and complete story.

Because junction heating could potentially contribute to the EQE droop,<sup>41</sup> we have measured the EQE curves under two conditions: (1) no deliberate junction temperature control, i.e., the device is simply sitting on a metal block, similar to the condition for the EL spatial mapping; (2) keeping the

junction temperature constant, using a technique developed recently.<sup>42</sup> Note that this approach is somewhat different from keeping the heat sink temperature constant because of the existence of a temperature gradient between the heat sink and the junction. For the first case, the junction temperature rises by about 35 °C for device A and 63 °C for device B at the highest current used ( $\sim 1$  A). As shown in Fig. 6, the junction heating does contribute to the droop. The effect can be measured by the ratio of the two droop curves, shown in the right axis of Fig. 6 as heating effect. For device A, the reduction from the  $I_{max}$  to  $I_f=0.95$  A is about 10% or 0.1%/( $A/cm^2$ ), and for device B from the  $I_{max}$  to  $I_f=0.75$  A is about 5% or 0.077%/( $A/cm^2$ ). Junction heating may affect the EQE in at least two ways: thermalization induced carrier delocalization, and thermal enhancement of the nonradiative recombination. The magnitude of the droop rate due to heating is relatively small: slightly smaller than that reported for the device showing minimal droop rate,<sup>38</sup> but much smaller than that observed in most devices where the droop is of concern.

Figure 7 shows local EQE vs.  $I_f$  for the two devices, each with one typical bright and dark spot, measured under

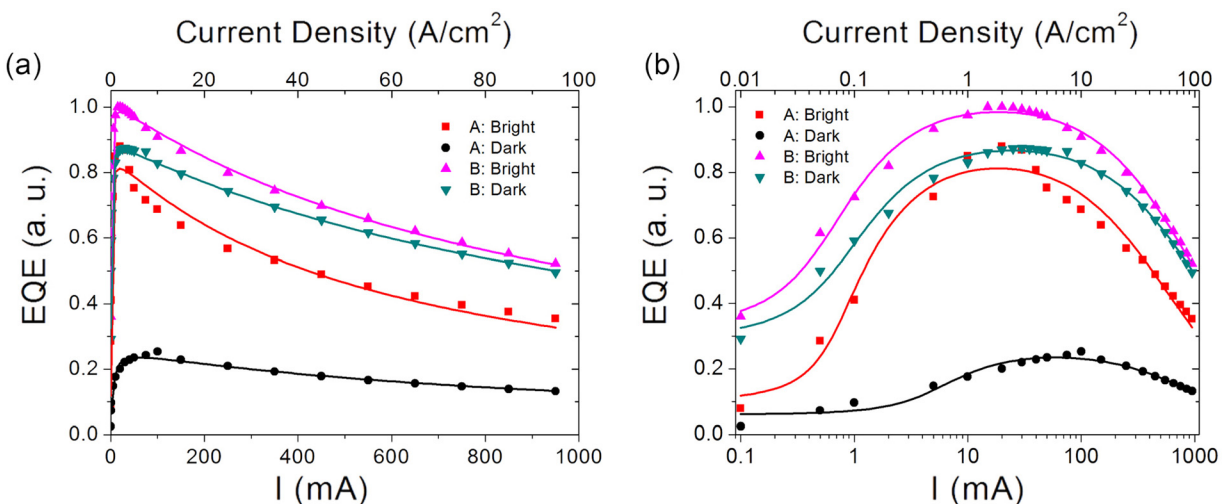


FIG. 7. Local EQE vs. current at selected locations for device A and B. Dots: the experimental data; solid lines: the fitting curves.

nominally same conditions. The curves are normalized to the peak intensity or EQE of the bright spot of device B. With the homogenous injection assumption mentioned above, the relative local EQE can be defined as the ratio of the local emission intensity and the injection current apart from a constant. It is clear that for device A, the curves for the bright and dark regions are drastically different: the bright region shows a rapid initial increase in EQE (large  $\tau_r$  or small  $I_{max}$ ) and high peak EQE but a fast decay (large  $\tau_{EQE}$ ), resembling the type II behavior, and the dark region a slow initial increase (small  $\tau_r$  or large  $I_{max}$ ) and low peak EQE but a slow decay (small  $\tau_{EQE}$ ), resembling type I. These two distinctly different droop behaviors have been frequently reported in the literature, but often measured from two independent devices and shown as normalized curves.<sup>7,13,21</sup> Obviously if the two curves for device A shown in Fig. 7 were normalized to the respective peak values, one would get a rather misleading conclusion that the dark region would be more desirable. For device B, the difference between the bright and dark spots is much smaller, and both are somewhat similar to the bright region of device A although the initial decay is not as fast.

In the literature, the EQE- $I_f$  curve is often described by an ABC model that includes nonradiative (A), radiative (B), and Auger (C) recombination.<sup>2,43</sup> In this model, EQE is not an explicit function of  $I_f$  but through the dependence of the carrier density on  $I_f$ , and the roles of PDs and EDs are not distinguished. We have recently proposed an alternative model that directly relates the EQE to  $I_f$ .<sup>31</sup> There we only used it to discuss the rise portion of the EQE- $I_f$  curve, to emphasize the significance of the rise part in the whole process of droop. This is a two-level model with one representing the band edge states that

contribute to the band edge emission, and the other mimicking the microscopic defect states relatively far away from the band edge states and the carriers there may recombine either radiatively or nonradiatively. Now we extend this model to cover the whole EQE curve by introducing an additional nonradiative loss mechanism to the states responsible for the LED emission, therefore, is able to model the droop process. It replaces the nonradiative recombination in the ABC with two contributions: PDs and EDs, and without the Auger term. We have two rate equations:<sup>31</sup>

$$\begin{cases} \frac{dn}{dt} = G - nW - n\gamma_t N_t (1-f) \\ \frac{dN}{dt} = n\gamma_t N_t (1-f) - fN_t W_t \end{cases}, \quad (1)$$

where  $n$  represents the electron density for the “band edge level,” including both localized and delocalized states,  $N$  for the electron density of the deep defect level with a defect density  $N_t$ ,  $G$  the generation or injection rate which is proportional to  $I_f$ ,  $W = W_r + W_{nr}$  is the total recombination rate for the band edge state, with  $W_r$  for radiative and  $W_{nr}$  for the additional nonradiative processes, such as the carrier capture by the EDs, that is expected to be enhanced by carrier delocalization,  $\gamma_t$  the defect capture coefficient with  $c_t = \gamma_t N_t$  the capture rate,  $f = N/N_t$  the defect occupation fraction,  $W_t$  the deep defect recombination rate. Carrier localization may suppress both  $c_t$  (through reducing  $N_t$ ) and  $W_{nr}$  (through reducing carrier mobility). The steady state solutions of Eq. (1) give rise to the equation below for the internal efficiency

$$\eta = \frac{nW_r}{G} = \frac{1}{2(1+\phi)} \left( 1 - \frac{\alpha(1+\phi) + \beta}{G} + \sqrt{\left( 1 + \frac{\alpha(1+\phi) + \beta}{G} \right)^2 - \frac{4\beta}{G}} \right), \quad (2)$$

where  $\alpha = W_r W_t / \gamma_t$ ,  $\beta = N_t W_t$ , and  $\phi = W_{nr} / W_r$ .  $\alpha$  may be understood as the effective recombination rate of the band edge level,  $\beta$  represents the maximum recombination rate of the defect level. This result is very similar to that derived for the low injection level,<sup>31</sup> except for the  $(1+\phi)$  term that depends on the injection level. When  $\beta = 0$  (with  $N_t = 0$ ) or  $\alpha \gg \beta$  (with  $W_r / c_t \gg 1$ ), Eq. (2) leads to  $\eta = (1+\phi)^{-1}$ . Furthermore, for sufficiently large  $G$  (e.g.,  $G \rightarrow 40\beta$ ),  $\eta \rightarrow (1+\phi)^{-1}(1-\beta/G)$ . To fit the relative experimental EQE, we rewrite Eq. (2) as

$$\eta = \frac{nW_r}{\zeta I_f} = \frac{C}{(1+\phi' I_f)} \left( 1 - \frac{\alpha'(1+\phi' I_f) + \beta'}{I_f} + \sqrt{\left( 1 + \frac{\alpha'(1+\phi' I_f) + \beta'}{I_f} \right)^2 - \frac{4\beta'}{I_f}} \right), \quad (3)$$

where  $G$  is replaced by  $\zeta I_f$ ,  $\alpha$ ,  $\beta$ , and  $\phi$  by  $\alpha' = \alpha/\zeta$ ,  $\beta' = \beta/\zeta$  and  $\phi' = \phi/I_f$ , and  $1/2$  by  $C$  to include the extraction efficiency. Equation (3) can then be used to fit the experimental data shown in Fig. 7. The value of  $\beta'$ , in the same unit as  $I_f$ , is a direct measure of the current required to saturate the

microscopic defects, roughly at  $40\beta'$ . The fitted curves are showed in solid lines that match well with the original data, and the fitting parameters are given in Table I. For device A, the dark region has a much larger  $\beta$  value than the bright region, indicating the existence of large density or effective

TABLE I. The fitting parameters of the two-level mode.

| Parameters     | Sample A              |                       | Sample B              |                       |
|----------------|-----------------------|-----------------------|-----------------------|-----------------------|
|                | Bright                | Dark                  | Bright                | Dark                  |
| $\alpha'$ (mA) | $7.62 \times 10^{-2}$ | 1.01                  | $1.68 \times 10^{-1}$ | $2.40 \times 10^{-1}$ |
| $\beta'$ (mA)  | $5.63 \times 10^{-1}$ | 3.38                  | $3.48 \times 10^{-1}$ | $4.88 \times 10^{-1}$ |
| $\phi'$        | $1.72 \times 10^{-3}$ | $1.03 \times 10^{-3}$ | $1.02 \times 10^{-3}$ | $8.44 \times 10^{-4}$ |

non-radiative centers in the dark region. For the other three cases, the  $\beta$  values are in the same order of magnitude, as reflected as their  $I_{max}$  values in Fig. 7. In the dark region of A, it is the large  $\beta$  that prevents the EQE to reach a high value, because the local PD density is so large they could not be saturated easily even when  $I_f$  approaches 100 mA or 10 A/cm<sup>2</sup>. The most important reason for the low EQE of the dark region is the large  $\beta$  value, leading to very efficient recombination loss through the deep defect states that are hard to saturate even at a moderately high injection level 10 A/cm<sup>2</sup>. A reasonable explanation would be that in the dark region, the carriers are more mobile, thus more susceptible to the PDs, which leads to the smaller peak EQE and larger  $I_{max}$ , whereas in the bright region, the carriers are more localized, thus more immune from the PDs, leading to the larger EQE and smaller  $I_{max}$ . This understanding is supported by the comparison of emission peak energy vs.  $I_f$  shown in Fig. 5(b): for the bright region, a significant blue shift or state filling occurs in roughly the 20–400 mA range, corresponding to the current range showing the fast droop, reflecting a progressive delocalization process; for the dark region, lacking of efficient localization prevents any observable blue shift. A similar correlation between the EL peak shift, leading to the carrier delocalization, and droop is also observed for device B, as shown in Fig. 5(c).

In Eq. (3), we have assumed  $W_{nr} \propto I_f$  although potentially other dependences are possible. As it is, at high current level, we have  $\text{EQE} \propto 1/(1 + \phi'I_f)$ , which is qualitatively similar to the ABC model.  $W_{nr}$  describes the loss of the delocalized carriers, which may occur through either the recombination at the EDs or leaking out from the QWs, leading to the droop. It has very little effect in the low current region or the rise part of the curve. Roughly, the quantity  $\phi'I_f/(1 + \phi'I_f)$  describes the fraction of the EQE loss as a result of the droop. The model adopted in this work is apparently an overly simplified one to capture all the details of the dynamic process of the device operation, but it is able to describe the important underlying physics of the EQE droop.

### C. Discussions

There has been overwhelmed evidence for the concurrence of the delocalization and droop, which naturally led to the conclusion that the delocalization is the primary mechanism for the droop.<sup>21–26</sup> Furthermore, nonradiative recombination through defects were believed to be primarily responsible for the loss of the delocalized carriers<sup>21–26</sup> although one could not exclude other loss channels, for instance, carrier leakage.<sup>2</sup> We will first discuss the potential

effects of defects, in particular the different roles of PDs and EDs in the rise and decay portion of the EQE– $I_f$  curve whereas in the literature the defect types were usually not specified and the discussions were typically focused on the decay portion. The EQE– $I_f$  curve for a typical InGaN LED involves at least three processes: (1) the nonradiative process caused by PDs that are more important in the low current region because they limit the carrier mobility and thus diminish the effectiveness of the EDs, but usually can be saturated under a moderately high injection level.<sup>28</sup> (2) Carrier localization and delocalization effect that is more significant in InGaN QW based blue LEDs<sup>44</sup> than in the devices based on other alloys such as GaInP. Localization limits the effectiveness of both PDs and EDs.<sup>27,28</sup> Delocalization typically occurs at 2–10 A/cm<sup>2</sup> level, as indicated by the onset of the blue shift in EL peak energy, shown in Fig. 5. However, delocalization itself does not quench the radiative recombination efficiency, but the loss of these mobile carriers through other channels does. (3) EDs and other possible mechanisms that take away the carriers from the band edge states before they can radiatively recombine. Our analyses of the rise process reveal the pivotal role of the interplay of PDs and carrier localization in setting the initial rate of the efficiency rise and its peak value. The understanding of the droop lies in that what is (are) the primary causes for the loss of the carriers that occupy the more mobile states in the QW. Note that virtually all optoelectronic devices suffer from droop at high carrier density either by electrical or optical generation. For instance, the best single crystalline GaAs and Si solar cells achieve their maximum efficiency at around 100 sun with short-circuit currents about 3–4 A/cm<sup>2</sup>,<sup>45</sup> which is similar in the order of magnitude to that of the LED droop point.

Can Auger be the primary contributor to the droop? By noticing the fact that the droop starts at a fairly low current density (as low as 2 A/cm<sup>2</sup>), concurrent with the delocalization, it is highly unlikely that the Auger recombination could play a significant role at this relatively low injection level. Furthermore, the shape and magnitude of the droop curve depends strongly on the details of the device fabrication parameters whereas the Auger recombination rate is supposed to be an intrinsic property of the material. Apparently, some devices have shown very little droop yet with high peak EQE:  $\sim 0.15\%/(\text{Acm}^{-2})$  with 54.4% (Ref. 38) and  $\sim 0.1\%/(\text{Acm}^{-2})$  with 52%.<sup>46</sup> These superior devices do not show the sharp droop right after the peak observed in most devices, such as those studied in this work. We note that for the bright region in device A, the initial fast droop, as shown in Fig. 7, occurs in about the same current range where the emission peak shows significant blue shift or state filling, as shown in Fig. 5(b). It is then the state filling leads to the carrier delocalization, making them vulnerable to whatever the mechanism leading to the droop. A very recent report has indeed shown the concurrent appearance of the Auger electron emission and the onset of droop.<sup>47</sup> However, the direct evidence of that Auger effect is the sole primary mechanism responsible for droop is yet to be seen.

Another plausible droop mechanism has been the carrier leakage.<sup>2</sup> There are indeed evidences for the occurring of the

carrier leakage. However, to conclude that this was the sole primary mechanism relied on the dismissal of the contribution of the EDs.<sup>2</sup> Qualitative similarity in their EQE- $I_f$  curves between AlGaInP and InGaN LEDs has been used to argue that the carrier delocalization could not be responsible for the droop, because it is asserted that for AlGaInP the composition fluctuation is minimal and dislocation density is negligible.<sup>2</sup> Evidentially, carrier localization due to both alloy fluctuation and other mechanisms are quite significant even for the simpler system GaInP,<sup>48,49</sup> although perhaps to a less degree than in InGaN, which in fact explains the difference in the onset temperature at which the delocalization (rapid droop) occurs between the two systems.<sup>2</sup> Our recent study on a very high quality GaAs sample has shown that while at a low carrier density, PDs can reduce the carrier mobility thus the effectiveness of the EDs; however, PDs can be relatively easy to be saturated with increasing carriers, making EDs more effective and the dominant nonradiative recombination channels that cannot be saturated even at a very high carrier density.<sup>28</sup> There is also clear evidence that threading edge dislocations act as nonradiative recombination centers in the InGaN QW.<sup>50</sup> For those exceptional high performance devices showing high peak EQEs and low droop rates,<sup>38,46</sup> they do not exhibit the rapid droop after reaching the peak. A reasonable explanation would be that such materials are more uniform thus with less localization and in the meantime have low PD and ED densities rather than being less leakage. Although one cannot dismiss the contribution of the carrier leakage to the loss of delocalized carriers, there is no solid argument to dismiss the contribution of the EDs either. Since even in a high quality GaAs the ED remains highly effective at high carrier density, there is no reason to think that all those high density EDs in InGaN would be benign, unless further concrete theoretical or experimental evidences are available.

We would like to point out a previously not specifically recognized effect of the carrier localization. We note that for device A, even at the highest current, the bright region remains significantly more efficient than the dark region [by a factor of 2.7 as shown in Fig. 7(b)]. The difference could be interpreted as that the localization sites still hold a significant amount of the carriers even at a rather high current; and only those carriers spilling-over the energy traps are susceptible to the loss mechanism(s) leading to the droop.

Above discussion would suggest neither type I nor type II is the ideal option. One could envision a more desirable scenario: for a material with a low PD density and a not-so-high density of EDs ( $10^6 \text{ cm}^{-2}$  or lower), the EQE- $I_f$  curve will exhibit a fast rise to a high value followed by a slow droop with a small droop rate, for instance,  $<0.1\%/(\text{A}/\text{cm}^2)$ . The slow decay part at the high current region is presumably due to the third process mentioned above. Note that for the dark region of device A, although with rather low EQE, the average droop rate is also small,  $\tau_{EQE} \sim 0.6\%/(\text{A}/\text{cm}^2)$  for the whole range from  $I_{max} \sim 10 \text{ A}/\text{cm}^2$  to  $95 \text{ A}/\text{cm}^2$ , of which a significant portion,  $\sim 0.1\%/(\text{A}/\text{cm}^2)$ , could be due to the junction heating effect. The best reported value for  $\tau_{EQE}$  was approximately  $0.1\%/(\text{A}/\text{cm}^2)$  for a device with 52% peak EQE although with a relatively small active area and

measured at 1% duty cycle.<sup>46</sup> This number is comparable to the junction heating effect of device B when measured for the whole device,  $0.077\%/(\text{A}/\text{cm}^2)$ . The relatively small  $\tau_{EQE}$  for the dark region of device A could be understood as the “intrinsic” droop rate that is determined by the density of the EDs as well as the junction heating effect, if the material were uniform, i.e., without significant energy fluctuation. Note that even for the other three curves, despite the significant early droop, in the high current region the droop rates all seem to converge to some low values. These discussions suggest that the Auger effect is unlikely to be the primary killer of the EQE or the primary mechanism of the droop, in particular for those devices with the fast droop occurring at relatively low current level, for instance below  $10 \text{ A}/\text{cm}^2$ , which agrees with the analysis of Refs. 19 and 20. Furthermore, the droop rate remains small and nearly constant for a large current range, for instance, in the case of the dark region of device A,  $\sim 0.6\%/(\text{A}/\text{cm}^2)$  from  $10 \text{ A}/\text{cm}^2$  to  $100 \text{ A}/\text{cm}^2$ , as well as the above mentioned example in the literature with an even smaller droop rate and a larger current range,  $\sim 0.1\%/(\text{A}/\text{cm}^2)$  up to  $200 \text{ A}/\text{cm}^2$ .<sup>46</sup> These results are inconsistent to the expected dependence on the carrier density for the Auger process. Although ultimate solution for the droop effect would be to reduce the both the microscopic and extended defect densities and improve the uniformity of the active layer, a practical mitigation of the droop effect for a device expected to operate only at the moderate current level could be the design of a more effective localization scheme.

#### IV. SUMMARY AND CONCLUSION

By performing spatially resolved droop study on InGaN QW blue LEDs, we are able to examine various possible droop mechanisms without the potential ambiguity causing by the variation in device processing. We suggest that the EQE-current curve may reflect the interplay of three effects: nonradiative recombination through point defects, carrier localization due to either In composition or well width fluctuation, and nonradiative recombination of the extended defects. These three effects are common to many optoelectronics devices. The effect of the carrier leakage is expected to be qualitatively similar to that of the extended defects, which should be evaluated further. The interplay of these effects manifests as two extreme types of droop behaviors (I and II). For the type I behavior associated with small energy fluctuation, the initial rise rate of EQE depends on the density of microscopic defects that need to be saturated. The carrier diffusion is enhanced after the saturation of the microscopic defects. Once the carriers become mobile, the extended defects, which are less likely to be saturated, start to capture them and quench the EQE, and lead to the EQE droop, as observed in the dark region of our device A. However, the droop rate purely due to the extended defects is expected to be relatively low, depending on the defect density. For the type II behavior associated with significant energy fluctuation, the local energy minimums can provide carrier trapping sites, and help to suppress the carrier diffusion to the extended defects. However, once the delocalization effect, an activation process with increasing carrier

density and temperature, sets in at a moderately high current level, a relatively fast droop occurs, as observed for instance in our device B and the bright region of device A. With further increasing current, the droop rate will converge to a lower rate that is determined by the carrier diffusion to the extended defects, as observed in the dark region of the device A. The most desirable type, type III, should exhibit a fast rise and a slow decay. Some devices reported in the literature are already close to have this ideal dependence, for instance, with >50% peak EQE and <0.1%/(A/cm) droop rate. For the majority devices where localization effect is significant and relatively high density of defects exist, as far as the droop mechanism is concern, the apparent cause of droop is the delocalization effect. However, identifying the ultimate mechanism responding to the droop boils down to one question: what happens to the delocalized carriers? Auger recombination, an intrinsic loss mechanism, if playing any role at all at very high current level, such as approaching 100 A/cm<sup>2</sup>, should not be the major concern for the LED operated at lower current, given the fact that some devices do show very little droop, suggesting that droop is extrinsic in nature. Various other droop mechanisms proposed in the literature, such as polarization field, could be considered as secondary effects because they may affect the carrier localization and diffusion, thus, indirectly contribute to the droop process. Improving carrier localization could be a practical way to mitigate the droop at least for a device operating at a moderately high current, but ultimate solution would be to reduce the density of the extended defects to eliminate the high current droop and the microscopic defects to improve the low current performance.

## ACKNOWLEDGMENTS

The work at UNC-Charlotte was supported partially by Bissell Distinguished Professorship, MURI/ARO (DAAD19-01-1-0591), and DARPA/MTO (W911NF-11-2-0070); at Xiamen University in part by the Major Science and Technology Project between University-Industry Cooperation in Fujian Province under Grant No. 2011H6025, NSF project under Grant No. 11104230, and Key Project of Fujian Province under Grant No. 2012H0039. We thank Dr. Haruhisa Takiguchi and Dr. D. L.-S. Dang for helpful discussions and references, and Qiong Chen and Naili Yue for technical assistance.

- <sup>1</sup>J. M. Phillips, M. E. Coltrin, M. H. Crawford, A. J. Fischer, M. R. Krames, R. M. Mach, G. O. Mueller, Y. Ohno, L. E. S. Rohwer, J. A. Simmons, and J. Y. Tsao, *Laser Photon. Rev.* **1**, 307 (2007).
- <sup>2</sup>J. Cho, E. F. Schubert, and J. K. Kim, *Laser Photon. Rev.* **7**, 408 (2013).
- <sup>3</sup>A. Y. Kim, W. Götz, D. A. Seigerwald, J. J. Wierer, N. F. Gardner, J. Sun, S. A. Stockman, P. S. Martin, M. R. Krames, R. S. Kern, and F. M. Steranka, *Phys. Status Solidi A* **188**, 15 (2001).
- <sup>4</sup>J. Piprek, *Phys. Status Solidi A* **207**, 2217 (2010).
- <sup>5</sup>Y. C. Shen, G. O. Mueller, S. Watanabe, N. F. Gardner, A. Munkholm, and M. R. Krames, *Appl. Phys. Lett.* **91**, 141101 (2007).
- <sup>6</sup>M. Zhang, P. Bhattacharya, J. Singh, and J. Hinckley, *Appl. Phys. Lett.* **95**, 201108 (2009).
- <sup>7</sup>Z. Q. Liu, T. B. Wei, E. Q. Guo, X. Y. Yi, L. C. Wang, J. X. Wang, G. H. Wang, Y. Shi, I. Ferguson, and J. M. Li, *Appl. Phys. Lett.* **99**, 091104 (2011).

- <sup>8</sup>A. Laubsch, M. Sabathil, W. Bergbauer, M. Strassburg, H. Lugauer, M. Peter, S. Lutgen, N. Linder, K. Streubel, J. Hader, J. V. Moloney, B. Pasenow, and S. W. Koch, *Phys. Status Solidi C* **6**, S913 (2009).
- <sup>9</sup>N. F. Gardner, G. O. Mueller, Y. C. Shen, G. Chen, S. Watanabe, W. Götz, and M. R. Krames, *Appl. Phys. Lett.* **91**, 243506 (2007).
- <sup>10</sup>E. Kioupakis, P. Rinke, K. T. Delaney, and C. G. Van de Walle, *Appl. Phys. Lett.* **98**, 161107 (2011).
- <sup>11</sup>K. T. Delaney, P. Rinke, and C. G. Van de Walle, *Appl. Phys. Lett.* **94**, 191109 (2009).
- <sup>12</sup>J. I. Shim, D. P. Han, H. Kim, D. S. Shin, G. B. Lin, D. S. Meyaard, Q. F. Shan, J. Cho, E. F. Schubert, H. Shim, and C. Sone, *Appl. Phys. Lett.* **100**, 111106 (2012).
- <sup>13</sup>B. J. Ahn, T. S. Kim, Y. Q. Dong, M. T. Hong, J. H. Song, J. H. Song, H. K. Yuh, S. C. Choi, D. K. Bae, and Y. Moon, *Appl. Phys. Lett.* **100**, 031905 (2012).
- <sup>14</sup>M. H. Kim, M. F. Schubert, Q. Dai, J. K. Kim, E. F. Schubert, J. Piprek, and Y. Park, *Appl. Phys. Lett.* **91**, 183507 (2007).
- <sup>15</sup>T. V. Rozhansky and D. A. Zakheim, *Phys. Status Solidi A* **204**, 227 (2007).
- <sup>16</sup>S. P. Chang, C. H. Wang, C. H. Chiu, J. C. Li, Y. S. Lu, Z. Y. Li, H. C. Yang, H. C. Kuo, T. C. Lu, and S. C. Wang, *Appl. Phys. Lett.* **97**, 251114 (2010).
- <sup>17</sup>X. Li, X. Ni, J. Lee, M. Wu, Ü. Ozgüür, H. Morkoç, T. Paskova, G. Mulholland, and K. R. Evans, *Appl. Phys. Lett.* **95**, 121107 (2009).
- <sup>18</sup>C. Huh, J. M. Lee, D. J. Kim, and S. J. Park, *J. Appl. Phys.* **92**, 2248 (2002).
- <sup>19</sup>J. Hader, J. V. Moloney, and S. W. Koch, *Appl. Phys. Lett.* **96**, 221106 (2010).
- <sup>20</sup>J. Hader, J. V. Moloney, and S. W. Koch, *Appl. Phys. Lett.* **99**, 181127 (2011).
- <sup>21</sup>J. X. Wang, L. Wang, W. Zhao, Z. B. Hao, and Y. Luo, *Appl. Phys. Lett.* **97**, 201112 (2010).
- <sup>22</sup>T. Mukai, M. Yamada, and S. Nakamura, *Jpn. J. Appl. Phys.* **38**, 3976 (1999).
- <sup>23</sup>N. I. Bochkarev, V. V. Voronenkov, R. I. Gorbunov, A. S. Zubrilov, P. E. Latyshev, Yu. S. Lelikov, Yu. T. Rebane, A. I. Tsyuk, and Yu. G. Shreter, *Semiconductors* **46**, 1032 (2012).
- <sup>24</sup>N. I. Bochkarev, Y. T. Rebane, and Y. G. Shreter, *Appl. Phys. Lett.* **103**, 191101 (2013).
- <sup>25</sup>T. J. Badcock, S. Hammersley, D. W. Parris, P. Dawson, M. J. Godfrey, M. J. Kappers, C. McAleese, R. A. Oliver, and C. J. Humphreys, *Jpn. J. Appl. Phys.* **52**, 08JK10 (2013).
- <sup>26</sup>J. Mickevicius, G. Tamulaitis, M. Shur, M. Shatalov, J. Yang, and R. Gaska, *Appl. Phys. Lett.* **103**, 011906 (2013).
- <sup>27</sup>Y. Zhang, M. D. Sturge, K. Kash, B. P. Van der Gaag, A. S. Gozdz, L. T. Florez, and J. P. Harbison, *Phys. Rev. B* **51**, 13303 (1995).
- <sup>28</sup>T. H. Gfroerer, Y. Zhang, and M. W. Wanlass, *Appl. Phys. Lett.* **102**, 012114 (2013).
- <sup>29</sup>S. H. Han, D. Y. Lee, H. W. Shim, G. C. Kim, Y. S. Kim, S. T. Kim, S. J. Lee, C. Y. Cho, and S. J. Park, *J. Phys. D: Appl. Phys.* **43**, 354004 (2010).
- <sup>30</sup>J. R. Xu, M. F. Schubert, A. N. Noemaun, D. Zhu, J. K. Kim, E. F. Schubert, M. H. Kim, H. J. Chung, S. Yoon, C. Sone, and Y. Park, *Appl. Phys. Lett.* **94**, 011113 (2009).
- <sup>31</sup>Y. Lin, Y. Zhang, Z. Q. Liu, L. Q. Su, J. H. Zhang, T. B. Wei, and Z. Chen, *Appl. Phys. Lett.* **101**, 252103 (2012); *Erratum: Appl. Phys. Lett.* **103**, 119902 (2013).
- <sup>32</sup>Y. Zhang, M. D. Sturge, K. Kash, B. P. Van der Gaag, A. S. Gozdz, L. T. Florez, and J. P. Harbison, *J. Lumin.* **60/61**, 400 (1994).
- <sup>33</sup>S. De, A. Layek, A. Raja, A. Kadir, M. R. Gokhale, A. Bhattacharya, S. Dhar, and A. Chowdhury, *Adv. Funct. Mater.* **21**, 3828 (2011).
- <sup>34</sup>M. Meneghini, S. Vaccari, N. Trivellin, D. D. Zhu, C. Humphreys, R. Butendheich, C. Leirer, B. Hahn, G. Meneghesso, and E. Zanoni, *IEEE Trans. Electron Devices* **59**, 1416 (2012).
- <sup>35</sup>J. Q. Xie, X. F. Ni, Q. Fan, R. Shimada, Ü. Özgüür, and H. Morkoç, *Appl. Phys. Lett.* **93**, 121107 (2008).
- <sup>36</sup>G. Chen, M. Craven, A. Kim, A. Munkholm, S. Watanabe, M. Camras, W. Götz, and F. Steranka, *Phys. Status Solidi A* **205**, 1086 (2008).
- <sup>37</sup>M. R. Krames, O. B. Shchekin, R. Mueller-Mach, G. O. Mueller, L. Zhou, G. Harbers, and M. G. Craford, *J. Display Technol.* **3**, 160 (2007).
- <sup>38</sup>Y. Narukawa, M. Sano, T. Sakamoto, T. Yamada, and T. Mukai, *Phys. Status Solidi A* **205**, 1081 (2008).
- <sup>39</sup>G. Tamulaitis, J. Mickevicius, D. Dobrovolskas, E. Kuokstis, M. Shur, M. Shatalov, J. Yang, and R. Gaska, *Phys. Status Solidi C* **7**, 1869 (2010).
- <sup>40</sup>S. Sonderegger, E. Feltin, M. Merano, A. Crottini, J. F. Carlin, R. Sachot, B. Deveaud, N. Grandjean, and J. D. Ganière, *Appl. Phys. Lett.* **89**, 232109 (2006).

- <sup>41</sup>C. L. Chao, R. Xuan, H. H. Yen, C. H. Chiu, Y. H. Fang, Z. Y. Li, B. C. Chen, C. C. Lin, C. H. Chiu, Y. D. Guo, H. C. Kuo, J. F. Chen, and S. J. Cheng, *IEEE Photon. Technol. Lett.* **23**, 798 (2011).
- <sup>42</sup>Y. Lin, Y. L. Gao, Y. J. Lu, L. H. Zhu, Y. Zhang, and Z. Chen, *Appl. Phys. Lett.* **100**, 202108 (2012).
- <sup>43</sup>D. Saguatti, L. Bidinelli, G. Verzellesi, M. Meneghini, G. Meneghesso, E. Zanoni, R. Butendeich, and B. Hahn, *IEEE Trans. Electron Devices* **59**, 1402 (2012).
- <sup>44</sup>S. F. Chichibu, A. Uedono, T. Onuma, B. A. Haskell, A. Chakraborty, T. Koyama, P. T. Fini, S. Keller, S. P. DenBaars, J. S. Speck, U. K. Mishra, S. Nakamura, S. Yamaguchi, S. Kamiyama, H. Amano, I. Akasaki, J. Han, and T. Sota, *Nat. Mater.* **5**, 810 (2006).
- <sup>45</sup>M. A. Green, K. Emery, Y. Hishikawa, W. Warta, and E. D. Dunlop, *Prog. Photovoltaics* **20**, 12 (2012).
- <sup>46</sup>Y. Zhao, S. Tanaka, C. C. Pan, K. Fujito, D. Feezell, J. S. Speck, S. P. DenBaars, and S. Nakamura, *Appl. Phys. Express* **4**, 082104 (2011).
- <sup>47</sup>J. Iveland, L. Martinelli, J. Peretti, J. S. Speck, and C. Weisbuch, *Phys. Rev. Lett.* **110**, 177406 (2013).
- <sup>48</sup>Y. Zhang, A. Mascarenhas, S. Smith, J. F. Geisz, J. M. Olson, and M. Hanna, *Phys. Rev. B* **61**, 9910 (2000).
- <sup>49</sup>B. Fluegel, S. Smith, Y. Zhang, A. Mascarenhas, J. F. Geisz, and J. M. Olson, *Phys. Rev. B* **65**, 115320 (2002).
- <sup>50</sup>D. Cherns, S. J. Henley, and F. A. Ponce, *Appl. Phys. Lett.* **78**, 2691 (2001).